# Competitive Solvation-Induced Interphases Enable Highly Reversible Zn Anodes

Leilei Zheng, Huihua Li, Xi Wang, Zhen Chen, Chen Hu, Kaidi Wang, Gaoli Guo, Stefano Passerini,* and Huang Zhang*

**ABSTRACT: Aqueous Zn-metal batteries have been recognized as promising energy storage devices due to their high theoretical energy density and cost-effectiveness. However, side reactions and Zn dendrite growth during cycling limit their practical application. Herein, we investigated methylammonium acetate as an electrolyte additive to enhance the reversibility and stability of the Zn anode. The results revealed that the acetate anions would competitively engage the $Zn^{2+}$ solvation structure to reduce the water reactivity and promote the anion-enriched structure in the electrolyte, which can efficiently suppress the byproducts and dendrite formation. These occurs thanks to the formation of an anion-derived, robust solid electrolyte interphase with an inorganic/organic hybrid structure. Such an electrolyte enables a long cycle life over 2000 h in the Zn||Zn cell and a high Coulombic efficiency of >99.5% for 700 cycles in the Zn||Ti cell. Therefore, both Zn||$Na_3V_2(PO_4)_3$ batteries and Zn||activated carbon capacitors in this electrolyte exhibit improved cycling performance.**

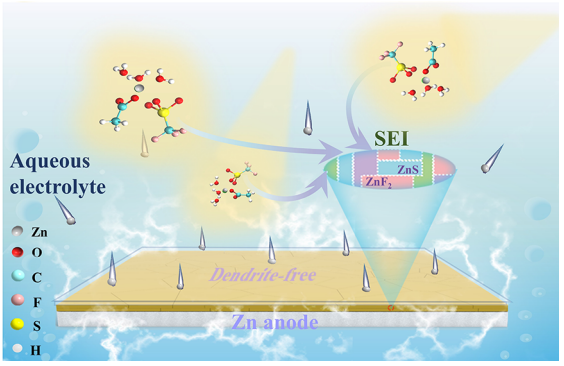


Aqueous zinc−metal batteries (AZBs) hold great promise as an efficient and safe energy storage technology for large-scale application, benefiting from the high energy of metallic zinc (Zn), intrinsic nonflammability, and cost-efficiency of aqueous electrolytes.[1] Additionally, the use of aqueous electrolytes can simplify the battery fabrication process, which can further reduce the manufacturing cost. However, the inferior reversibility of the Zn anode, mainly caused by dendrite growth, interfacial parasitic reactions, and water-related side reactions, remains as one of the crucial challenges restricting the further development and commercial exploitation of AZBs.[2] The dendrite formation originates from the uneven distribution of $Zn^{2+}$ and nucleation of Zn on the anode surface, which is known as the "tip effect".[3] To circumvent these issues, extensive efforts have been devoted including designing 3D current collectors,[4,5] building artificial interphases on the Zn anode,[6,7] and optimizing the electrolytes components.[8,9] For example, by introducing a Bi-based energizer on the Zn metal surface, the resultant Zn/Bi electrode not only circumvents Zn dendrite growth but also improves Zn anode anticorrosion performance.[10] In our recent work, an artificial $ZnF_2$ layer on the Zn anode surface was developed to address the side reaction and dendrite growth issues in a mild electrolyte.[11] Besides, the electrolyte modulation strategy is an easy and efficient approach to improve the Zn anode, which can reshape the solvation structures, decrease the reactivity of water, and *in situ* induce the unique interphase chemistry.[12,13] Highly concentrated electrolytes have been reported to effectively break the hydrogen bond network and weaken the solvation interaction between $H_2O$ and $Zn^{2+}$, thus significantly decreasing the water activity.[14] However, their high cost and high viscosity are considered as main drawbacks for practical applications.[15,16]

Additive engineering has been demonstrated as an effective strategy, capable of simultaneous regulation of the solvation structure and electrode interface, thus improving the reversibility of the Zn anode.[17,18] In fact, various additives have been introduced into aqueous Zn-electrolytes, such as organic solvents,[19,20] polymers,[21] inorganic salts,[22,23] and supermolecules.[24,25] For example, simultaneous regulation of cations and anions was achieved by adding $NaClO_4$ salts as additives in the $ZnSO_4$ electrolyte, which can form a protective layer to eliminate the anode's adverse effects and lessen cathode dissolution.[26] Learning from the nonaqueous lithium dendrite inhibition strategies, developing an ionic additive has

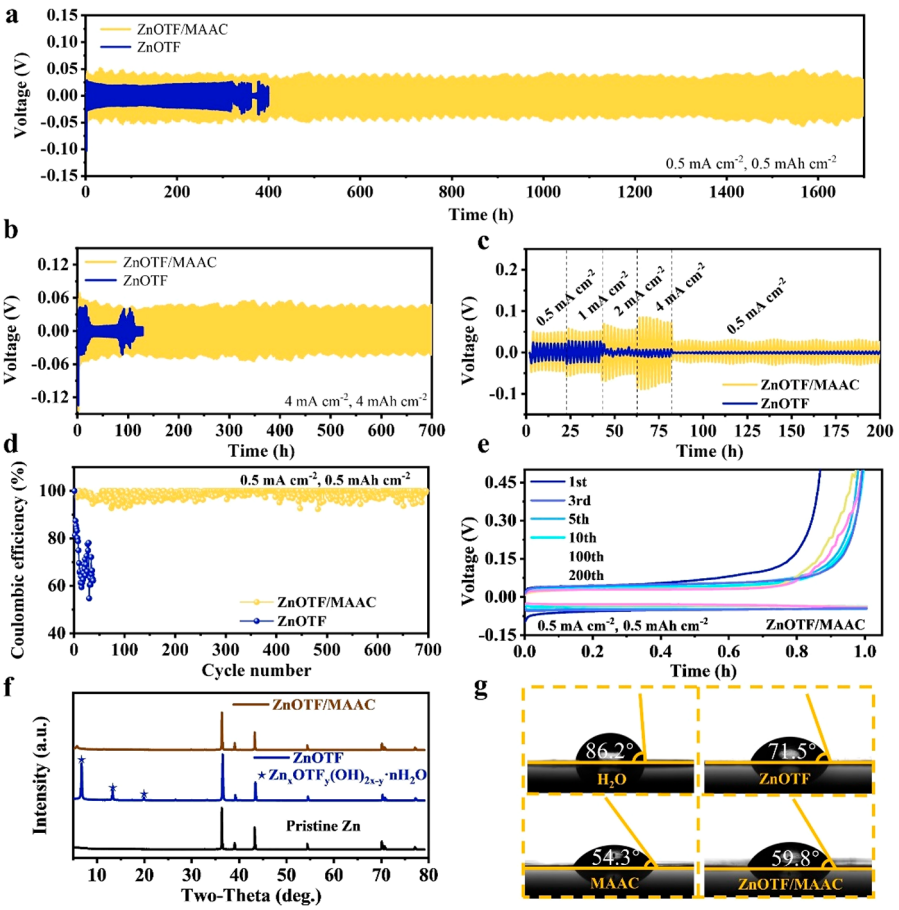


**Figure 1. Reversibility of the Zn anodes in the ZnOTF and ZnOTF/MAAC electrolytes. Long-term stripping/plating profiles of Zn||Zn symmetric cells (a) at 0.5 mA cm$^{-2}$ and 0.5 mAh cm$^{-2}$ and (b) at 4 mA cm$^{-2}$ and 4 mAh cm$^{-2}$. (c) Rate performance of Zn||Zn symmetric cells. (d) Coulombic efficiencies (CEs) of Zn plating/stripping in the Zn||Ti cells at 0.5 mA cm$^{-2}$ and 0.5 mAh cm$^{-2}$. (e) Typical galvanostatic voltage profiles of the Zn||Ti cell in the ZnOTF/MAAC electrolyte at 0.5 mA cm$^{-2}$ and 0.5 mAh cm$^{-2}$. (f) XRD patterns of Zn electrodes reobtained from Zn||Zn symmetric cells after 20 cycles. (g) Contact angle measurements of $H_2O$, MAAC, the ZnOTF electrolyte, and the ZnOTF/MAAC electrolyte on the Zn foils.**

been proved to be a promising approach that would effectively regulate the Zn deposition behavior in AZBs.[17,27,28] Typically, a diluted aqueous electrolyte, i.e., 4 mol kg$^{-1}$ (molality: "m") of Zn trifluoromethanesulfonate (ZnOTF) with 0.5 m trimethylethylammonium trifluoromethanesulfonate ($Me_3EtNOTF$) as the additive, was proposed by Wang et al., which engenders *in situ* formation of a fluorinated and hydrophobic interphase and enables a highly reversible Zn metal anode.[29] Recently, a cationic surfactant-type additive, tetrabutylammonium sulfate ($TBA_2SO_4$), was introduced into the $ZnSO_4$ electrolyte to improve the Zn anode for AZBs.[30] The $TBA^+$ cations would electrostatically adsorb and aggregate in the vicinity of protuberances to create the protective $TBA^+$ layers, leading to the dendrite-free homogeneous Zn deposition. Similarly, the quaternary triethylmethylammonium (TMA) cation has been added as an ionic additive into diluted $ZnCl_2$ and $ZnSO_4$ electrolytes.[31] During the plating process, the cation favors the homogeneous Zn deposition via adsorbing onto the Zn metal surface, thus inhibiting the formation of byproducts and dendritic growth. Overall, the functionality of these cationic additives is to reduce the nucleation overpotential and activation energy of Zn plating, alleviate dendritic growth, and lower the water reactivity.

However, most of the as-proposed ionic additives share the same anions with the zinc salts used in the electrolyte. Since the solid electrolyte interphase (SEI) formation in aqueous electrolytes is basically involving the decomposition of the anions and water, introducing an anionic additive would be a feasible approach to preferentially regulate the SEI components and protect the Zn anode.[32] More generally, introducing an additional anion (with the ionic additive) can also affect the solvation structure, influence the desolvation energy and ion transport kinetics, and facilitate the formation of a robust anion-derived SEI layer.[33]

Herein, we introduce methylammonium acetate (MAAC) as an ionic additive in dilute ZnOTF electrolytes to achieve the byproduct-free and dendrite-free aqueous Zn metal anode. Theoretical simulations and experimental techniques evidence that MAAC enables a reconstruction of the solvation structure of cations and anions in an aqueous electrolyte, in which the acetate anions competitively participate in the $Zn^{2+}$ primary solvation sheath. Meanwhile, the preferentially adsorbed $OTF^-$ anions would be electroreduced to form an inorganic/organic hybrid SEI layer on Ti and Zn surfaces. These characteristics endow higher CE and reversibility of Zn plating/stripping in Zn||Zn cells and Zn||Ti cells. Therefore, the reversibility of Zn||$Na_3V_2(PO_4)_3$ (NVP) batteries and Zn||activated carbon (AC) capacitors can be significantly improved by this electrolyte.

Symmetric Zn||Zn cells were fabricated to investigate the reversibility of the Zn anodes in 2 m ZnOTF (denoted as

ZnOTF) and 2 m ZnOTF with 5 wt % MAAC (denoted as ZnOTF/MAAC) electrolytes. Long-term galvanostatic cycling tests were conducted at different areal current densities and capacities. As shown in Figure 1a, the cell using ZnOTF/MAAC displays stable cycling for 1700 h at 0.5 mA $cm^{-2}$ and 0.5 mAh $cm^{-2}$ with an average overpotential of 40 mV. However, the cell employing the ZnOTF electrolyte exhibits a short-circuit after 320 h. In addition, the MAAC-containing cells display long-term cycling stability over 2000 h at a higher current (1 mA $cm^{-2}$) and capacity (1 mAh $cm^{-2}$) (Figure S1, Supporting Information). When the current densities increase, the cell in the ZnOTF electrolyte shows exacerbated cycling stability. Particularly, when cycled at 4 mA $cm^{-2}$ and 4 mAh $cm^{-2}$, the cell employing the MAAC additive displays excellent stability over 700 h with an ca. 60 mV overpotential (Figure 1b). In striking contrast, the Zn||Zn symmetric cells in ZnOTF show a short circuit after only a few cycles, confirming that the presence of MAAC significantly improves the reversibility and stability of Zn-deposition, especially at high rates. Further, the Zn||Zn symmetric cells were also cycled at more harsh conditions of 10 mA $cm^{-2}$ and 10 mAh $cm^{-2}$, referring to a depth-of-discharge (DOD) of 56.9%. As illustrated (Figure S3), the cell in the ZnOTF electrolyte can only be cycled for 5 cycles, which is much less than that of the ZnOTF/MAAC electrolyte. Moreover, the rate performance of Zn||Zn cells in electrolytes with/without MAAC was also studied at various current densities ranging from 0.5 to 4 mA $cm^{-2}$ (Figure 1c). Clearly, the cell employing the ZnOTF/MAAC electrolyte delivers a steadier voltage profile than that using the baseline electrolyte. When the current was increased to 2 mA $cm^{-2}$, the cell using ZnOTF immediately fails. Besides, when the current density is turned back to 0.5 mA $cm^{-2}$, the Zn cell using the ZnOTF/MAAC electrolyte still works but delivers a lower overpotential, which can be explained by the decreased local current densities due to the surface structural change after cycling at higher current densities, which is commonly observed in both aqueous zinc metal batteries and nonaqueous lithium metal batteries.[8,34,35] However, the cell in ZnOTF does not operate, further proving the beneficial effect of MAAC as an ionic additive to significantly inhibit the dendrite growth upon Zn plating and enable high reversibility at high current density.

To further illustrate the reversibility of Zn plating/stripping behavior, Zn||Ti asymmetric cells were assembled. Figure 1d presents the Coulombic efficiencies (CEs) of the cells cycled under 0.5 mA $cm^{-2}$ and 0.5 mAh $cm^{-2}$. The CEs of the asymmetric cell in the ZnOTF/MAAC electrolyte exhibit a slight decrease followed by an increase to 99.8% in the initial 40 cycles and finally stabilize at >99.5% for 700 cycles (1400 h). In contrast, the Zn||Ti cell employing the ZnOTF baseline electrolyte shows a fast CE decrease during the initial cycles and fails after 40 cycles. The voltage profiles in Figure 1e validate the highly reversible Zn plating/stripping behavior in the presence of the MAAC additive, as confirmed by the low and stable overpotential (about 30 mV at the 200th cycle) in contrast to the fluctuating stripping curves with higher overpotentials in the baseline electrolyte (Figure S2). To further illustrate the reversibility of Zn at high current density in the ZnOTF/MAAC electrolyte, the Zn||Zn symmetric cells were also cycled at 10 mA $cm^{-2}$ and 10 mAh $cm^{-2}$, which refers to a depth-of-discharge (DOD) of 56.9% (based on the Zn foil in a thickness of 30 $\mu$m). As illustrated in Figure S3, the cell in the ZnOTF electrolyte can only be cycled for 5 cycles (10 h), which is much less than that of ZnOTF/MAAC. These results clearly demonstrate the superior performance and positive role of the MAAC additive for the Zn anode.

The low cell overpotential, high CE, and long cycling life in the presence of MAAC may originate from the inhibited side reaction and inhibit the dendrite growth at Zn electrodes, which is also reflected by the stabilized interfacial behavior upon cycling (Figure S4). It should be noted that the impedance at low frequencies is not stable and the interfacial impedance is changing upon time, due to the potential degradation process. For example, if the corrosion process occurs, the imaginary part of the impedance becomes inductive (or negative). The nucleation and growth mechanisms are further analyzed by the chronoamperometry (CA) test. As shown in Figure S5, the electrode goes through the intractable 2D diffusion process and the 3D diffusion process successively under an overpotential of −150 mV. In the 2D diffusion process, Zn ions will steadily deposit and form dendrites at the position which are conducive to the charge transfer to minimize the surface energy and narrow exposure area ("tip" effect). In the 3D diffusion process, Zn ions will be reduced to Zn and form a smooth and dense Zn deposition layer in a place where the initial adsorption has occurred.[36] Compared with the baseline electrolyte, the Zn electrode in the ZnOTF/MAAC electrolyte displays lower 3D diffusion current density, revealing that Zn dendrite growth is effectively inhibited by the presence of MAAC to achieve stable Zn deposition.[37]

X-ray diffraction (XRD) patterns were collected on the Zn metal electrodes retrieved from the symmetric cells employing both electrolytes, after 20 cycles. As shown in Figure 1f, the XRD results clearly demonstrate the presence of $Zn_xOTF_y(OH)_{2x-y}{\cdot}nH_2O$ (ZOTFH) on the surface of the Zn electrode cycled in the ZnOTF electrolyte, which is regarded as the main product of $OH^-$ ions reacting with $ZnOTf_2$ and $H_2O$.[38,39] In contrast, there is no discernible byproduct observed on the Zn metal electrode cycled in the ZnOTF/MAAC electrolyte, suggesting that the additive can efficiently inhibit the byproduct formation during the Zn plating/stripping. Contact angle measurements were also employed to determine the wettability of $H_2O$, MAAC, the ZnOTF electrolyte, and the ZnOTF/MAAC electrolyte on Zn foils (Figure 1g). As seen, the intrinsic wettability of MAAC is superior to that of $H_2O$, indicating that MAAC components are more likely to adsorb on Zn surfaces. In fact, the contact angle significantly decreases from 71.5° in ZnOTF to 59.8° in ZnOTF/MAAC. The superior zincophilicity of the MAAC-containing electrolyte is expected to facilitate the homogeneous Zn deposition.[40,41]

In view of the suppressed byproduct formation and enhanced zincophilicity of the modified electrolyte, the reversibility of Zn plating/stripping is greatly improved in the MAAC-containing electrolyte. To further investigate the Zn deposition kinetics, the galvanostatic deposition was studied in more detail to examine the nucleation and growth behavior of Zn. Figure 2a presents the characteristic voltage profiles upon Zn plating on Ti current collectors employing ZnOTF and ZnOTF/MAAC electrolytes. As seen, the Zn nucleation overpotential ($\eta$) in the MAAC-based electrolyte (126.4 mV) is slightly higher than that recorded in the baseline electrolyte (109.7 mV), inducing a more fine-grained Zn nuclei growth with the MAAC additive.[42,43] In addition, the plateau potential in ZnOTF/MAAC is also higher than that in the ZnOTF electrolyte, which could be attributed to the occurring

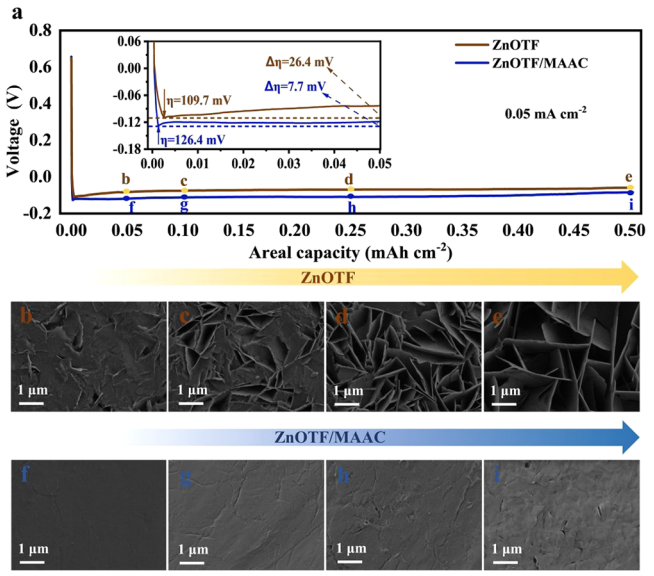


**Figure 2. Nanoscale nucleation and morphology evolution of plated Zn. (a) The first plating voltage profiles of Zn||Ti cells at 0.05 mA cm$^{-2}$ and 0.5 mAh cm$^{-2}$ with a magnified view of the initial nucleation process. SEM images of plated Zn on Ti in ZnOTF (b–e) and ZnOTF/MAAC (f–i) after (b and f) 0.05 mAh cm$^{-2}$, (c and g) 0.1 mAh cm$^{-2}$, (d and j) 0.25 mAh cm$^{-2}$, and (e and i) 0.5 mAh cm$^{-2}$, respectively.**

formation of the electrode–electrolyte interphase.[44,45] However, the difference between the plateau and nucleation overpotentials ($\Delta\eta$) is only 7.7 mV in the MAAC-containing electrolyte, i.e., about one-quarter of that in the baseline electrolyte, suggesting the favorable Zn growth on the existing Zn nuclei.

To track the morphology evolution of the Zn-plated Ti, ex situ scanning electron microscopy (SEM) images were recorded at selected deposited Zn amounts ranging from 0.05 mAh cm$^{-2}$ to 0.5 mAh cm$^{-2}$ (Figure 2b-i). In the electrolyte with the MAAC additive, the homogeneous deposition of Zn is observed, resulting from the fine Zn nuclei growth into dense and compact layers. By sharp contrast, layered flake-like growth occurs in the baseline electrolyte, with the size of the features growing with increased areal capacities. Particularly, the SEM images of 0.5 mAh cm$^{-2}$ plated Ti electrodes clearly illustrate the uniform morphology of the deposit achieved in ZnOTF/MAAC versus the flake-like deposits achieved in ZnOTF, confirming that the addition of MAAC enables an optimal Zn deposition.

The Zn plated on Ti electrodes after 20 cycles (at 0.5 mA cm$^{-2}$ and 0.5 mAh cm$^{-2}$) was further analyzed by SEM (Figure 3). The Zn deposit in the ZnOTF/MAAC electrolyte has a flat surface (Figure 3a and b), whereas a porous and dendritic morphology is observed in the one obtained in the ZnOTF electrolyte (Figure 3e and f). This is fully consistent with the rapid cell failure in both Zn||Zn and Zn||Ti cells (Figure 1a and d). The cross-sectional view of Zn deposition in ZnOTF shows a spongy morphology (Figure 3g and h), which is caused by the byproducts' formation (mainly ZOTFH) occurring together with the Zn deposition. On the other hand, a dense Zn layer is observed in the MAAC-containing electrolyte (Figure 3c and d), consistently with the result observed during the initial cycle (Figure 2). *In situ* optical microscopy was used to intuitively investigate the Zn deposition behavior on bare Zn at a current density of 10 mA cm$^{-2}$, as presented in Figure

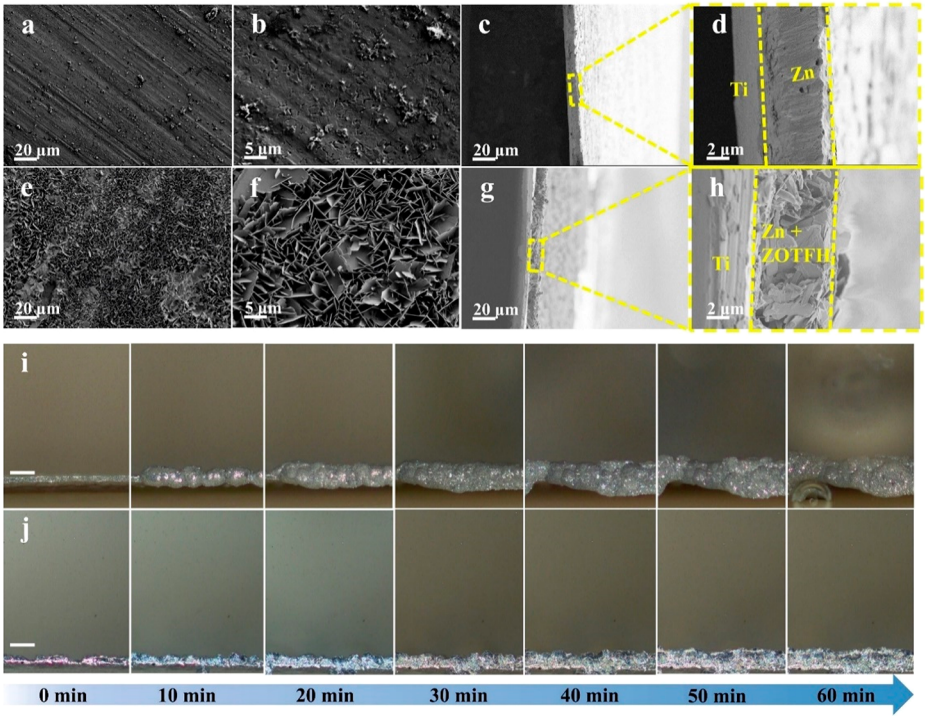


**Figure 3. Morphology evolution of plated Zn in the electrolytes. (a–d) SEM images of Zn-plated Ti in ZnOTF/MAAC: (a and b) top view and (c and d) cross-sectional view. (e–h) SEM images of Zn-plated Ti in ZnOTF: (e and f) top view and (g and h) cross-sectional view. *In situ* optical microscopy images of the cross-sectional Zn deposition morphology on the Zn foil with plating times in the (i) ZnOTF and (j) ZnOTF/MAAC electrolytes at 10 mA cm$^{-2}$. The scale bar is 100 $\mu$m.**

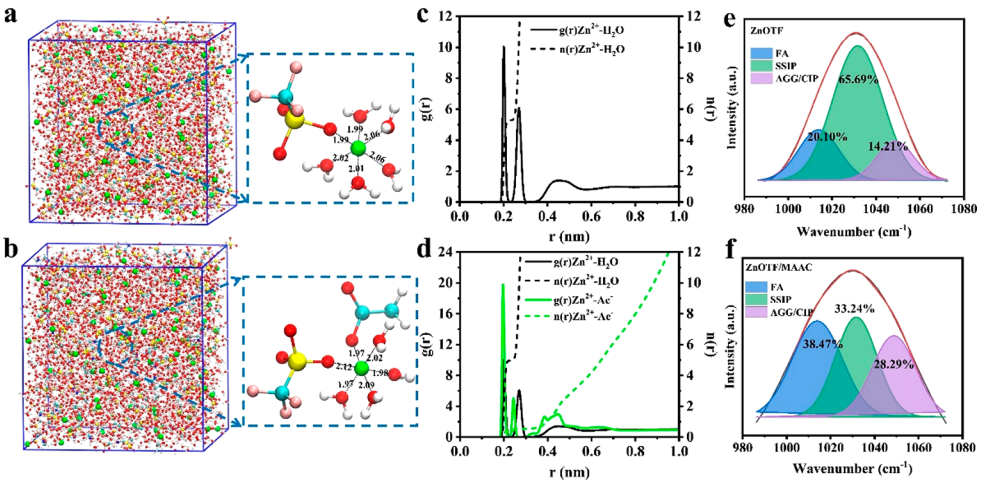


**Figure 4. Solvation structure analysis in the aqueous electrolytes. 3D snapshots of the simulated solvation structures in the (a) ZnOTF and (b) ZnOTF/MAAC electrolytes. Radial distribution function [g(r)] and corresponding integrated coordination numbers [n(r)] obtained from MD simulation of the (c) ZnOTF and (d) ZnOTF/MAAC electrolytes. (e, f) Raman spectra in the wavenumber region of the $SO_3$ stretching modes.**

3i, j. It is clearly seen that a number of protuberances appear after a plating of 10 min and continuously grow in the ZnOTF electrolyte along with lots of bubbles observed during the plating process, indicating the dendrite growth and water decomposition. In contrast, the Zn deposition behavior in the ZnOTF/MAAC electrolyte shows a relatively uniform thickness without obvious dendrites in the whole plating process.

The solvation structure is expected to have a significant impact on regulating the Zn deposition kinetics and interfacial behavior. In fact, the notion that the bulk properties of an electrolyte, such as the degree of hydrogen bonding interaction and the state of the ion-pairs, significantly affect the morphologies of deposits is well accepted. The solvation structures of these two electrolytes were investigated by molecular dynamics (MD). In an aqueous Zn-based electrolyte, the conventional classification of solvation structures is based on the characteristics of the anions' interactions with $Zn^{2+}$, including the free anion (FA), solvent-separated ion pair (SSIP), contact ion pair (CIP), and aggregate (AGG).[15,16] Distinctively, as shown in partially enlarged detail (Figure 4a, b), the Zn cation is used as the center to define the solvates according to the number of anions. For the solvent surrounded $Zn^{2+}$ (SSZ), cations are captured by water molecules, implying that anions interact with water through hydrogen bonds rather than coordinate with $Zn^{2+}$. The $Zn^{2+}$-anion single pair (ZASP) and $Zn^{2+}$-anion cluster (ZAC) are defined considering one and more than one anions are coordinated in the primary solvation sheath, respectively.[32,46] In the ZnOTF-based electrolyte, SSZ is the dominant solvate species (Figure 4a). Also, ZASP is observed in which one $OTf^-$ anion participates in the $Zn^{2+}$ primary solvation sheath. In the ZnOTF/MAAC electrolyte, however, $Ac^-$ anions are present in addition to water molecules and $OTf^-$ anions, which could be in close contact with $Zn^{2+}$, resulting in a highly increased content of ZAC with respect to the ZnOTF electrolyte, even though the involvement of $Ac^-$ in the solvation structure slightly changes the hydrogen bond networks, as depicted in the partial enlarged snapshots (Figure 4b).

To quantitatively analyze the solvation structure of $Zn^{2+}$, the radial distribution functions (RDFs) and coordination number (CN) distribution functions based on MD simulations were conducted in the ZnOTF and ZnOTF/MAAC aqueous electrolytes. In the former electrolyte (Figure 4c), a sharp peak of Zn−$H_2O$ at about 2.0 Å is observed, while a transition state between the CIP and SSIP appears at 2.7 Å. The average coordination number is 5.30. The radial distribution function g(r) profile of the $Zn^{2+}$-$OTF^-$ (Figure S6a) reveals a sharp peak at 1.98 Å, indexed to the $Zn^{2+}$ coordination with $OTF^-$ by O in the primary solvation sheath. When MAAC is added in the electrolyte (Figure 4d), sharp peaks at 1.96 and 2.44 Å appear, associated with the $Zn^{2+}$ coordination with $Ac^-$ anions by O, suggesting that these anions are involved in the primary solvation sheath of the $Zn^{2+}$ cations. This is due to the $Ac^-$ anion being a stronger H-bonding acceptor with water.[47] Thus, the involvement of $OTF^-$ anions in the first solvation shell of $Zn^{2+}$ is reduced (Figure S4b and Figure 4b). The average coordination number of Zn in the MAAC-based electrolyte is 4.97, which is 6.2% lower than that of the baseline electrolyte and, thus, can only result from the $Ac^-$ anion in the solvation structure. As reported, the coordination of $Zn^{2+}$ with $H_2O$ favors hydrogen evolution upon zinc plating, which releases a large amount of $OH^-$ resulting in the byproduct ZOTFH (Figure 1f).[48] Compared to the baseline ZnOTF solution, the presence of MAAC decreases the number of $H_2O$ molecules surrounding the $Zn^{2+}$ cation, resulting in the suppressed water reactivity and facilitated $Zn^{2+}$ transport. Noteworthy, the long-range spatial correlation of the $CH_3NH_3^+$ cation with $OTF^-$, $Ac^-$, and $H_2O$ molecules can be distinguished, as shown in Figure S7, where the broader peaks imply the weaker interaction between these oppositely charged ions.[49] However, a corresponding sharpening of the cation−anion peak at around 4.0 Å indicates that $CH_3NH_3^+$-$Ac^-$ pairs tend to aggregate more closely than $CH_3NH_3^+$-$OTF^-$ pairs.[50]

According to the above theoretical calculations, the anions, including both $OTF^-$ and $Ac^-$, are involved in the solvation structure of $Zn^{2+}$. The coordination states of $OTF^-$ anions in the MAAC-based electrolyte were experimentally verified by Raman spectroscopy. The full-range Raman spectra of the electrolytes are displayed in Figure S8. The amplified profiles in Figure S9 exhibit the vibrations of $-CH_3$ and $-NH_3$ groups from the MAAC additive in the electrolyte. The $-SO_3$ stretching modes are analyzed in detail, and the results are

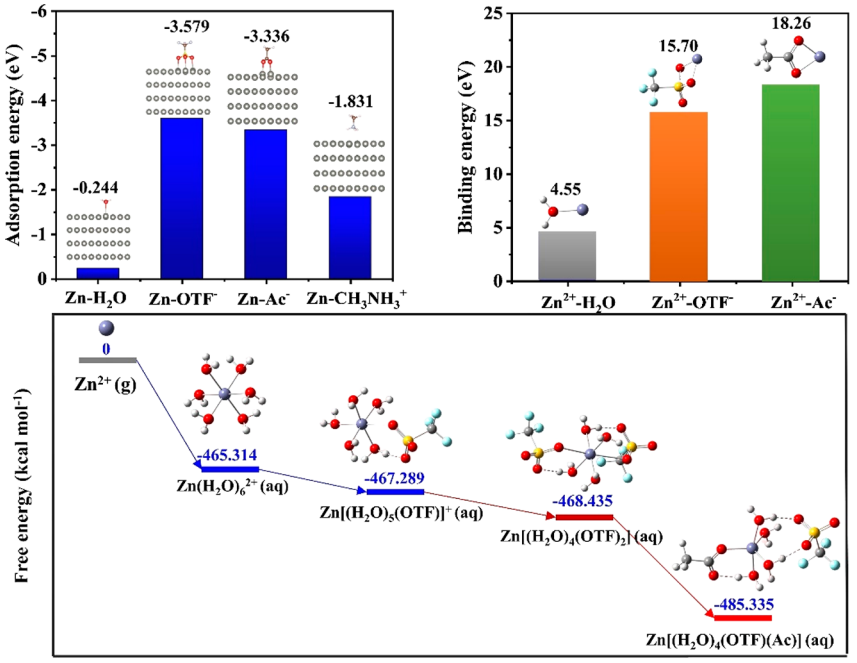


**Figure 5. Theoretical understanding of the roles of anions on Zn plating/stripping. (a) The adsorption energy of $H_2O$, $OTF^-$, $Ac^-$, and $CH_3NH_3^+$ on the Zn(002) substrate. (b) The binding energies (b) between two ingredients in the electrolytes of $Zn^{2+}$-$Ac^-$, $Zn^{2+}$-$OTf^-$, and $Zn^{2+}$-$H_2O$. (c) The free energy change in the transformation process of anion-involved solvation structures.**

presented in Figure 4e and f. The deconvoluted results yield three Gaussian components, which can be assigned to the FA, SSIP, and CIP/AGG portions. It is found that with the MAAC additive, the content of SSIP decreases sharply to 33.24%, while the portion of AGG and CIP increases from 14.21% to 28.29%. Since the solvation structure transformation is conducive to the reduction of anionic complexes, the strong coordination between the anions and cations endows the formation of a functional SEI on the electrode.[51,52] By contrary, water would preferentially be decomposed to construct a loose layer in the ZnOTF electrolyte, which leads to the low reversibility of Zn plating/stripping and rapid formation of the byproduct of ZOTFH.

Fourier-transform infrared spectroscopy (FTIR) was also conducted to analyze the changes of hydrogen bonding in these two electrolytes (Figure S10). Following the considerations on the H−O stretching band as a function of established hydrogen bonds, the three Gaussian components were correspondingly assigned to the dominating populations of $H_2O$ molecules, that is, "network water" (NW), "intermediate water" (IW), and "multimer water" (MW) molecules.[53,54] As shown in Figure S11, the variations of the respective populations illustrate that "network water" is the main population in these two electrolytes, while its proportion slightly increases from 73.4% to 76.4% upon addition of MAAC into the ZnOTF solution. Liquid NMR data have been performed on the electrolytes. The $^1H$ NMR spectra of these two electrolytes are shown in Figure S12, and the chemical shift of $^1H$ from $H_2O$ is only associated with the presence of ZnOTF. Besides, with the added MAAC in the electrolyte, the chemical shift of $^1H$ from $H_2O$ did not show an obvious change, revealing that $Ac^-$ anions mainly interact with $Zn^{2+}$ in the primary solvation sheath due to the high binding energy of $Zn^{2+}$-$Ac^-$.[55] These results clearly evidence that the competitive $Ac^-$ anions will participate in the solvation structure, replacing the water molecules in the primary solvation sheath, resulting in the efficiently suppressed decomposition of water molecules, e.g., hydrogen evolution.

DFT calculations were further performed to verify the interactions within the electrolyte species as well as the $Zn^{2+}$-solvation environment. First, to understand the adsorption energies of $H_2O$, $OTF^-$, $Ac^-$, and $CH_3NH_3^+$ on the Zn(002) surface were computed. As seen in Figure 5a, the adsorption energy of $OTF^-$ on Zn is −3.597 eV, lower than those of $H_2O$ (−0.244 eV), $Ac^-$ (−3.336 eV) and $CH_3NH_3^+$ (−1.831 eV). The lower adsorption energies of anions indicate that the $OTF^-$ and $Ac^-$ anions preferentially adsorb on the Zn surface and exclude the $H_2O$ molecules in the inner Helmholtz plane, which are peculiarly prone to form the anion-derived SEI layer, thus inhibiting the water decomposition and dendrite growth.[8,32] The binding energies (Figure 5b) between two ingredients in electrolytes follow an order of $Zn^{2+}$-$Ac^-$ (18.26 eV) > $Zn^{2+}$-$OTf^-$ (15.70 eV) > $Zn^{2+}$-$H_2O$ (4.55 eV), which suggests that $Ac^-$ anions can competitively participate in the $Zn^{2+}$ primary solvation sheath. Considering the free energies via DFT calculations, the desolvation of $Zn(H_2O)_6^{2+}$ needs to overcome a high energy barrier of 465.3 kcal $mol^{-1}$ (Figure 5c). When the $Ac^-$ and $OTF^-$ substitute for the $H_2O$, the lower-energy $Zn[(H_2O)_4(OTF^-)(Ac^-)]$ is formed. And the energy difference of 20.0 kcal $mol^{-1}$ allows the transformation process in thermodynamics. Compared with the typical $Zn^{2+}$ solvation structure of $Zn(H_2O)_6^{2+}$, the anion-involved solvation structure has a higher desolvation energy, which intensifies the desolvation energy barriers and increases the overpotential for stripping-plating. However, the $Zn^{2+}$-$Ac^-$ and $Zn^{2+}$-$OTF^-$ units enable the anion-enrichment interface, and the preferentially absorbed $OTF^-$ anions on the Zn surface would facilitate the reductive anion decomposition, which are conducive to the formation of an interphase layer on the electrode surface.[40]

The nucleation and deposition of $Zn^{2+}$ strongly depend on the properties of the anode/electrolyte interface induced by

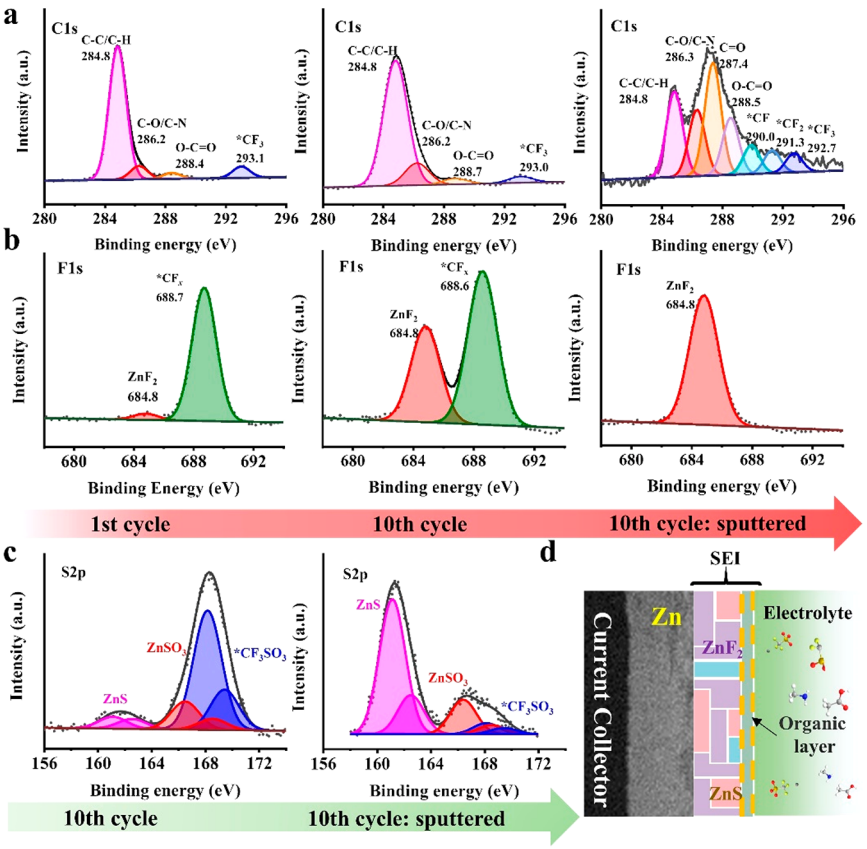


**Figure 6. Analysis of the solid-electrolyte interphases on the Zn-plated Ti substrates, retrieved from the Zn||Ti cell cycled at 1 mA cm$^{-2}$ in the ZnOTF/MAAC electrolyte. (a) XPS C 1s spectra, (b) F 1s spectra after 1 cycle, after 10 cycles, and at a depth of 10 nm after sputtering. (c) XPS S 2p spectra after 10 cycles and at a depth of 10 nm after sputtering. (d) Schematic of the SEI structure formed on the Zn-plated Ti electrode.**

the critical anion−cation coordination. To reveal the protective mechanism, the solid electrolyte interphase (SEI) on the cycled Ti electrode retrieved from the asymmetric Zn||Ti cells in ZnOTF/MAAC was investigated by X-ray photoelectron spectroscopy (XPS). Initially, the carbon species were analyzed on the Ti electrode as displayed in Figure 6a. At the initial plated state, the C 1s spectrum demonstrates a dominant peak located at ~284.8 eV, which is assigned to the C−H/C−C species. In view of the potential components available in the electrolyte, it is mostly contributed from $Ac^-$ anions absorbed on the surface. In addition, other peaks are detected and assigned (~293.0 eV for $CF_3$, ~286.2 eV for C−O/C−N, and ~288.4 eV for O═C−O). The surface component on the Ti after the 10th plating is similar to that of the first cycle. After sputtering by $Ar^+$ for 10 min, relatively low-intensity signals from the carbon species remain due to the removal of most organic species. However, additional peaks located at ~290.0 eV and ~291.3 eV can be observed, which can be attributed to the existence of CF and $CF_2$ species, evidencing the decomposition of $OTF^-$ anions after the Zn stripping/plating process. The F 1s spectra further confirm the anion-induced layer formation on the electrode surface (Figure 6b). As seen, the fluorine-based species in the Zn-plated electrode after the first cycle are mostly the organic $CF_3$ compound (~688.7 eV), while only a trace amount of inorganic $ZnF_2$ (~684.8) is detected, suggesting the outer layer of the SEI is mainly composed of organic species. After 10 cycles, the distinctive peak related to the inorganic $ZnF_2$ increases, indicating the continuous decomposition of $OTF^-$ anions during the initial cycles. After 10 min of sputtering, only $ZnF_2$ is found, indicating the formation of a $ZnF_2$-rich interphase. It should be noted that the N species related to the $CH_3NH_3^+$ cation are rarely detected in both fresh and sputtered Ti electrodes after cycling (Figure S13), which indicates the low involvement of the cation from the additive in the SEI formation. Interestingly, by analyzing the high-resolution S 2p spectra, it is found that the inner-SEI layer (after sputtering) consists of mainly inorganic ZnS and trace amount of $ZnSO_3$, as illustrated in Figure 6c. Summarily, these results concretely evidence the formation of an inorganic fluoride- and sulfide-rich ($ZnF_2$ and ZnS) SEI induced by the $OTF^-$ anion decomposition in the electrolyte with the MAAC additive, as schematically illustrated in Figure 6d. Such an interphase can suppress dendrite growth by promoting $Zn^{2+}$ migration and deposition and prevent parasitic reactions during Zn plating.

To give evidence on the SEI nature on the cycled Zn metal anode, FIB-TEM with energy-dispersive X-ray spectroscopy (EDX) mapping was performed, as presented in Figure S14. The EDX mapping results reveal the main constituent elements of SEI are C, F, O, and S from $OTF^-$ anions on the surface of the Zn anode. The HR-TEM images in Figure S15 show the ZnS and $ZnF_2$ nanocrystals with distinct lattice planes embedded in the amorphous matrix, revealing the presence of both inorganic crystalline and organic components of the SEI after Zn plating. XPS was also carried out on the surface of plated Zn retrieved from the Zn||Zn symmetric cell after 10 cycles and at a depth of ~10 nm underlying the surface by removing the upper components via 10 min of $Ar^+$

sputtering (Figure S16). Before sputtering, the C 1s spectrum exhibits the similar components with the species on Ti, indicating the existence of organic species. The F 1s spectrum on the surface exhibits two major components: $ZnF_2$ (at 684.8 eV) and $*CF_x$ organic species (at 688.8 eV). The S 2p signal can be ascribed to the precipitation of $OTF^-$ anions along with minor ZnS and $ZnSO_3$ species. These results are in accordance with the Ti substrates. However, at a depth of ~10 nm (sputtering for 10 min), the organic species in both F 1s and S 2p spectra reduce, while the $ZnF_2$ and ZnS fractions increase with lower intensities compared with those on the Ti substrate, indicating the diversity of the interphase structure on the Zn substrate. Identifying the exact effect from the substrates for SEI formation is beyond the scope of this work and will be part of a future study. The N 1s spectra show relatively weak intensity and even disappear after sputtering, which confirms the electrochemical stability of cations from MAAC. These results further confirm that $OTF^-$ anions are key to the formation of SEI.

As a more general proof-of-concept, the diluted electrolyte system containing 1 m ZnOTF and 0.25 m ZnAc (denoted as 1 m ZnOTF + 0.25 m ZnAc) was prepared. The asymmetric Zn||Cu cells were fabricated and cycled at conditions of 0.5 mA $cm^{-2}$ and 0.5 mAh $cm^{-2}$, as presented in Figure S17. In the diluted ZnOTF baseline electrolyte, the Zn||Cu cell exhibits rather poor reversibility. However, in the presence of $Ac^-$ anions, the cell exhibits much improved cycling stability with high Coulombic efficiencies (in an average value of 98.9%), which is higher than those of 1 m ZnOTF and 2 m ZnOTF electrolytes. These results strongly evidence the profound role of $Ac^-$ anions in stabilizing the Zn stripping/plating.

To illustrate the feasibility of such a proposed ZnOTF/MAAC electrolyte in energy storage devices based on Zn metal electrochemistry, Zn||NVP full cells were assembled as a proof of concept. The $Na^+$-extracted NVP serves as an efficient host for multivalent Zn cations via a quasi-two-stage intercalation.[56] The XRD pattern confirms the crystal structure of NVP (Figure S18), and the SEM image shows its porous morphology with crystalline NVP particles embedded in the carbon framework. The cell configuration is illustrated in Figure S19a. Figure S19b displays the initial galvanostatic charge−discharge (GCD) curves of Zn||NVP cells in the ZnOTF and ZnOTF/MAAC electrolytes at 50 mA $g^{-1}$. The cell with the baseline electrolyte delivered a specific charging capacity exceeding 200 mAh $g^{-1}$ but a rather low initial CE of 40.7%. In sharp contrast, the Zn||NVP cell using the ZnOTF/MAAC electrolyte exhibits a distinct charging plateau with a specific capacity of 99.9 mAh $g^{-1}$ and an initial CE of 93.5%. The long-term cycling stabilities of Zn||NVP batteries were performed. The GCD profile at the 50th cycle (Figure S19c) clearly demonstrates significant voltage changes for the cell with ZnOTF, which can be essentially attributed to the inevitable decomposition of NVP cathodes.[57] However, no obvious differences are observed in the charging and discharging plateaus of the cell with ZnOTF/MAAC at the 50th and even 300th cycles (Figure S19d). Based on a long-term cycling test at 50 mA $g^{-1}$ (Figure S20), this cell shows superior stability with a capacity retention of 64% and an average CE of 99.6% for 300 cycles. The long-term cycling stability of the NVP material as a cathode in an aqueous electrolyte is still a challenge, especially considering the inevitable material dissolution at a low current rate.[58] In this respect, further material modification is required to suppress the capacity decay. On the other hand, the cell employing ZnOTF showed fast capacity decay and CE deterioration. To verify the contribution of the interface/interphase, impedance measurements were recorded on the cells employing both the electrolytes before and after cycling, as presented in Figure S21. The fitted results are listed in Table S1. The fresh cell in ZnOTF/MAAC shows lower bulk resistance (Rs) and charge transfer resistance (Rct) than those of ZnOTF. After cycling, both cells display reduced charge transfer resistance (Rct), while the one in ZnOTF/MAAC possesses a much lower Rct value and a distinct interphase resistance (Rf), which can be explained by the formation of robust SEI layers. The improved cycling stability and interfacial behaviors of Zn||NVP batteries in the ZnOTF/MAAC electrolyte clearly show that MAAC improves the reversibility of Zn stripping/plating in Zn-based aqueous batteries.

To demonstrate the versatility of this proposed electrolyte, a hybrid and more sustainable energy storage device was tested, based on the Zn metal (negative electrode) and commercial activated carbon (AC, positive electrode) (Figure S22a). Based on charge, the anions are physically adsorbed on the AC electrode, while $Zn^{2+}$ cations are electrochemically deposited at the negative electrode. The subsequent discharge process involves the reversed processes. Such chemistry, making use of sustainable materials and high-power capability, is considered very promising for large-scale, high-power applications; however, its deployment has always been hindered by the poor Zn reversibility.[59,60] The typical GCD profiles of the hybrid capacitors are shown in Figure S22b-c. As seen, the initial CE of the device is remarkably improved in ZnOTF/MACC, benefiting from the high reversibility of the Zn anode in such an electrolyte. The long-term cycling results (Figure S23) further confirm that the MAAC-containing electrolyte enables the Zn||AC capacitor much prolonged stability over 3000 cycles at a high current density of 2 A $g^{-1}$. In contrast, a short-circuit occurs in the cell employing ZnOTF, resulting from the dendritic growth at the Zn electrode. As generally known, since the activated carbon electrode based on electrochemical double layer capacitive behavior is relatively reversible and stable, the failure of the hybrid capacitor mainly results from the deterioration of the Zn metal electrode.[60] Indeed, electrochemical impedance spectroscopy (EIS) results before and after cycling (Figure S24) show the higher impedance of the cell in ZnOTF than that of the MAAC-based electrolyte, related to the reversibility of the Zn metal electrode. These results further evidence the superior feasibility of such an electrolyte for advanced energy storage devices based on Zn metal electrochemistry.

In summary, methylammonium acetate, added as a sustainable ionic additive to the aqueous zinc triflate electrolyte, promotes the reversibility of the Zn anode. The use of this additive enables the byproduct-free and dendrite-free Zn plating/stripping in both symmetric Zn||Zn and asymmetric Zn||Ti cells yielding to high Coulombic efficiencies and long cycling stability. Theoretical and spectroscopic results revealed that the competitive participation of $Ac^-$ anions in the $Zn^{2+}$ primary solvation sheath leads to an anion-enriched structure, which can effectively reduce the water activity and boost the formation of a robust, anion-derived SEI. Taking advantage of the high reversibility of Zn plating/stripping in the MAAC-containing electrolyte, the cycling stability of Zn||$Na_3V_2(PO_4)_3$ batteries and Zn||activated carbon capacitors is remarkably improved. Our findings offer a basic understanding

on regulating the anion-derived SEI by the competitive anions in the solvation structure and will give insights into developing sustainable and diverse advanced aqueous electrolytes for Zn electrochemistry.

## ASSOCIATED CONTENT

### Data Availability Statement

The data that support the findings of this study are available from the corresponding author upon reasonable request.

## AUTHOR INFORMATION


### Corresponding Authors

**Stefano Passerini** − *Helmholtz Institute Ulm (HIU), D-89081 Ulm, Germany; Karlsruhe Institute of Technology (KIT), D-76021 Karlsruhe, Germany; Chemistry Department, Sapienza University of Rome, 00185 Rome, Italy;* orcid.org/0000-0002-6606-5304; Email: stefano.passerini@kit.edu

**Huang Zhang** − *Institute of Flexible Electronics, Northwestern Polytechnical University, Xi'an 710072, China;* orcid.org/0000-0002-7695-261X; Email: iamhzhang@nwpu.edu.cn

### Authors

**Leilei Zheng** − *Institute of Flexible Electronics, Northwestern Polytechnical University, Xi'an 710072, China*

**Huihua Li** − *Helmholtz Institute Ulm (HIU), D-89081 Ulm, Germany; Karlsruhe Institute of Technology (KIT), D-76021 Karlsruhe, Germany*

**Xi Wang** − *Key Laboratory of Engineering Dielectric and Applications (Ministry of Education), School of Electrical and Electronic Engineering, Harbin University of Science and Technology, Harbin 150080, PR China*

**Zhen Chen** − *Key Laboratory of Engineering Dielectric and Applications (Ministry of Education), School of Electrical and Electronic Engineering, Harbin University of Science and Technology, Harbin 150080, PR China;* orcid.org/0000-0002-5199-0935

**Chen Hu** − *Institute of Flexible Electronics, Northwestern Polytechnical University, Xi'an 710072, China*

**Kaidi Wang** − *Institute of Flexible Electronics, Northwestern Polytechnical University, Xi'an 710072, China*

**Gaoli Guo** − *Institute of Flexible Electronics, Northwestern Polytechnical University, Xi'an 710072, China*


### Notes

The authors declare no competing financial interest.

## ACKNOWLEDGMENTS


This work was financially supported by the Natural Science Basic Research Program of Shaanxi (2021JQ-110), the Natural Science Foundation of China (Grant No. 52277215), the Natural Science Foundation of Chongqing (cstc2020jcyj-msxmX0667), Fundamental Research Funds for the Central Universities, and the Helmholtz Association within the Network of Excellence on post-Lithium batteries (ExNet-0035). The authors would also like to acknowledge Xinxin Kang and Prof. Lin Song for their help in the synthesis of MAAC.


## REFERENCES


(1) Tang, B.; Shan, L.; Liang, S.; Zhou, J. Issues and Opportunities Facing Aqueous Zinc-Ion Batteries. *Energy Environ. Sci.* **2019**, *12* (11), 3288−3304.

(2) Zampardi, G.; La Mantia, F. Open Challenges and Good Experimental Practices in the Research Field of Aqueous Zn-Ion Batteries. *Nat. Commun.* **2022**, *13* (1), 687.

(3) Xie, F.; Li, H.; Wang, X.; Zhi, X.; Chao, D.; Davey, K.; Qiao, S.-Z. Mechanism for Zincophilic Sites on Zinc-Metal Anode Hosts in Aqueous Batteries. *Adv. Energy Mater.* **2021**, *11* (9), 2003419.

(4) An, Y.; Tian, Y.; Xiong, S.; Feng, J.; Qian, Y. Scalable and Controllable Synthesis of Interface-Engineered Nanoporous Host for Dendrite-Free and High Rate Zinc Metal Batteries. *ACS Nano* **2021**, *15* (7), 11828−11842.

(5) Cui, B.-F.; Han, X.-P.; Hu, W.-B. Micronanostructured Design of Dendrite-Free Zinc Anodes and Their Applications in Aqueous Zinc-Based Rechargeable Batteries. *Small Struct.* **2021**, *2* (6), 2000128.

(6) Guo, J.; Ming, J.; Lei, Y.; Zhang, W.; Xia, C.; Cui, Y.; Alshareef, H. N. Artificial Solid Electrolyte Interphase for Suppressing Surface Reactions and Cathode Dissolution in Aqueous Zinc Ion Batteries. *ACS Energy Lett.* **2019**, *4* (12), 2776−2781.

(7) Zhang, Q.; Su, Y.; Shi, Z.; Yang, X.; Sun, J. Artificial Interphase Layer for Stabilized Zn Anodes: Progress and Prospects. *Small* **2022**, *18* (40), 2203583.

(8) Huang, C.; Zhao, X.; Liu, S.; Hao, Y.; Tang, Q.; Hu, A.; Liu, Z.; Chen, X. Stabilizing Zinc Anodes by Regulating the Electrical Double Layer with Saccharin Anions. *Adv. Mater.* **2021**, *33* (38), 2100445.

(9) Xing, Z.; Huang, C.; Hu, Z. Advances and Strategies in Electrolyte Regulation for Aqueous Zinc-Based Batteries. *Coord. Chem. Rev.* **2022**, *452*, 214299.

(10) Wang, M.; Meng, Y.; Li, K.; Ahmad, T.; Chen, N.; Xu, Y.; Sun, J.; Chuai, M.; Zheng, X.; Yuan, Y.; Shen, C.; Zhang, Z.; Chen, W. Toward Dendrite-Free and Anti-Corrosion Zn Anodes by Regulating a Bismuth-Based Energizer. *eScience* **2022**, *2* (5), 509−517.

(11) Han, J.; Euchner, H.; Kuenzel, M.; Hosseini, S. M.; Groß, A.; Varzi, A.; Passerini, S. A Thin and Uniform Fluoride-Based Artificial Interphase for the Zinc Metal Anode Enabling Reversible Zn/$MnO_2$ Batteries. *ACS Energy Lett.* **2021**, *6* (9), 3063−3071.

(12) Cao, L.; Li, D.; Hu, E.; Xu, J.; Deng, T.; Ma, L.; Wang, Y.; Yang, X.-Q.; Wang, C. Solvation Structure Design for Aqueous Zn Metal Batteries. *J. Am. Chem. Soc.* **2020**, *142* (51), 21404−21409.

(13) Zhang, Q.; Luan, J.; Tang, Y.; Ji, X.; Wang, H. Interfacial Design of Dendrite-Free Zinc Anodes for Aqueous Zinc-Ion Batteries. *Angew. Chem., Int. Ed.* **2020**, *59* (32), 13180−13191.

(14) Wang, F.; Borodin, O.; Gao, T.; Fan, X.; Sun, W.; Han, F.; Faraone, A.; Dura, J. A.; Xu, K.; Wang, C. Highly Reversible Zinc Metal Anode for Aqueous Batteries. *Nat. Mater.* **2018**, *17*, 543−549.

(15) Yamada, Y.; Wang, J.; Ko, S.; Watanabe, E.; Yamada, A. Advances and Issues in Developing Salt-Concentrated Battery Electrolytes. *Nat. Energy* **2019**, *4* (4), 269−280.

(16) Zhang, H.; Liu, X.; Li, H.; Hasa, I.; Passerini, S. Challenges and Strategies for High-Energy Aqueous Electrolyte Rechargeable Batteries. *Angew. Chem., Int. Ed.* **2021**, *60* (2), 598−616.

(17) Guo, S.; Qin, L.; Zhang, T.; Zhou, M.; Zhou, J.; Fang, G.; Liang, S. Fundamentals and Perspectives of Electrolyte Additives for

Aqueous Zinc-Ion Batteries. *Energy Storage Mater.* **2021**, *34*, 545−562.
(18) Du, Y.; Li, Y.; Xu, B. B.; Liu, T. X.; Liu, X.; Ma, F.; Gu, X.; Lai, C. Electrolyte Salts and Additives Regulation Enables High Performance Aqueous Zinc Ion Batteries: A Mini Review. *Small* **2022**, *18* (43), 2104640.
(19) Dong, Y.; Miao, L.; Ma, G.; Di, S.; Wang, Y.; Wang, L.; Xu, J.; Zhang, N. Non-Concentrated Aqueous Electrolytes with Organic Solvent Additives for Stable Zinc Batteries. *Chem. Sci.* **2021**, *12* (16), 5843−5852.
(20) Liu, S.; Mao, J.; Pang, W. K.; Vongsvivut, J.; Zeng, X.; Thomsen, L.; Wang, Y.; Liu, J.; Li, D.; Guo, Z. Tuning the Electrolyte Solvation Structure to Suppress Cathode Dissolution, Water Reactivity, and Zn Dendrite Growth in Zinc-Ion Batteries. *Adv. Funct. Mater.* **2021**, *31* (38), 2104281.
(21) Banik, S. J.; Akolkar, R. Suppressing Dendrite Growth during Zinc Electrodeposition by PEG-200 Additive. *J. Electrochem. Soc.* **2013**, *160* (11), D519.
(22) Zhou, X.; Ma, K.; Zhang, Q.; Yang, G.; Wang, C. Highly Stable Aqueous Zinc-Ion Batteries Enabled by Suppressing the Dendrite and By-Product Formation in Multifunctional $Al^{3+}$ Electrolyte Additive. *Nano Res.* **2022**, *15* (9), 8039−8047.
(23) Xu, Y.; Zhu, J.; Feng, J.; Wang, Y.; Wu, X.; Ma, P.; Zhang, X.; Wang, G.; Yan, X. A Rechargeable Aqueous Zinc/Sodium Manganese Oxides Battery with Robust Performance Enabled by $Na_2SO_4$ Electrolyte Additive. *Energy Storage Mater.* **2021**, *38*, 299−308.
(24) Qiu, M.; Sun, P.; Wang, Y.; Ma, L.; Zhi, C.; Mai, W. Anion-trap Engineering toward Remarkable Crystallographic Reorientation and Efficient Cation Migration of Zn Ion Batteries. *Angew. Chem., Int. Ed.* **2022**, *61* (44), e202210979.
(25) Zhao, K.; Fan, G.; Liu, J.; Liu, F.; Li, J.; Zhou, X.; Ni, Y.; Yu, M.; Zhang, Y.-M.; Su, H.; Liu, Q.; Cheng, F. Boosting the Kinetics and Stability of Zn Anodes in Aqueous Electrolytes with Supramolecular Cyclodextrin Additives. *J. Am. Chem. Soc.* **2022**, *144* (25), 11129−11137.
(26) Wang, Z.; Zhou, M.; Qin, L.; Chen, M.; Chen, Z.; Guo, S.; Wang, L.; Fang, G.; Liang, S. Simultaneous Regulation of Cations and Anions in an Electrolyte for High-Capacity, High-Stability Aqueous Zinc−Vanadium Batteries. *eScience* **2022**, *2* (2), 209−218.
(27) Pan, B.; Lau, K.-C.; Vaughey, J. T.; Zhang, L.; Zhang, Z.; Liao, C. Ionic Liquid as an Effective Additive for Rechargeable Magnesium Batteries. *J. Electrochem. Soc.* **2017**, *164* (4), A902.
(28) Deyab, M. A. Ionic Liquid as an Electrolyte Additive for High Performance Lead-Acid Batteries. *J. Power Sources* **2018**, *390*, 176−180.
(29) Cao, L.; Li, D.; Pollard, T.; Deng, T.; Zhang, B.; Yang, C.; Chen, L.; Vatamanu, J.; Hu, E.; Hourwitz, M. J.; Ma, L.; Ding, M.; Li, Q.; Hou, S.; Gaskell, K.; Fourkas, J. T.; Yang, X.-Q.; Xu, K.; Borodin, O.; Wang, C. Fluorinated Interphase Enables Reversible Aqueous Zinc Battery Chemistries. *Nat. Nanotechnol.* **2021**, *16*, 902−910.
(30) Bayaguud, A.; Luo, X.; Fu, Y.; Zhu, C. Cationic Surfactant-Type Electrolyte Additive Enables Three-Dimensional Dendrite-Free Zinc Anode for Stable Zinc-Ion Batteries. *ACS Energy Lett.* **2020**, *5* (9), 3012−3020.
(31) Yao, R.; Qian, L.; Sui, Y.; Zhao, G.; Guo, R.; Hu, S.; Liu, P.; Zhu, H.; Wang, F.; Zhi, C.; Yang, C. A Versatile Cation Additive Enabled Highly Reversible Zinc Metal Anode. *Adv. Energy Mater.* **2022**, *12* (2), 2102780.
(32) Xu, X.; Su, H.; Zhang, J.; Zhong, Y.; Xu, Y.; Qiu, Z.; Wu, H. B.; Wang, X.; Gu, C.; Tu, J. Sulfamate-Derived Solid Electrolyte Interphase for Reversible Aqueous Zinc Battery. *ACS Energy Lett.* **2022**, *7*, 4459−4468.
(33) Zhang, Q.; Ma, Y.; Lu, Y.; Zhou, X.; Lin, L.; Li, L.; Yan, Z.; Zhao, Q.; Zhang, K.; Chen, J. Designing Anion-Type Water-Free $Zn^{2+}$ Solvation Structure for Robust Zn Metal Anode. *Angew. Chem., Int. Ed.* **2021**, *60* (43), 23357−23364.
(34) Feng, X.; Li, P.; Yin, J.; Gan, Z.; Gao, Y.; Li, M.; Cheng, Y.; Xu, X.; Su, Y.; Ding, S. Enabling Highly Reversible Zn Anode by Multifunctional Synergistic Effects of Hybrid Solute Additives. *ACS Energy Lett.* **2023**, *8* (2), 1192−1200.
(35) Wang, H.; Lin, D.; Xie, J.; Liu, Y.; Chen, H.; Li, Y.; Xu, J.; Zhou, G.; Zhang, Z.; Pei, A.; Zhu, Y.; Liu, K.; Wang, K.; Cui, Y. An Interconnected Channel-Like Framework as Host for Lithium Metal Composite Anodes. *Adv. Energy Mater.* **2019**, *9* (7), 1802720.
(36) Zhao, Z.; Zhao, J.; Hu, Z.; Li, J.; Li, J.; Zhang, Y.; Wang, C.; Cui, G. Long-Life and Deeply Rechargeable Aqueous Zn Anodes Enabled by a Multifunctional Brightener-Inspired Interphase. *Energy Environ. Sci.* **2019**, *12* (6), 1938−1949.
(37) Liu, Y.; Guo, T.; Liu, Q.; Xiong, F.; Huang, M.; An, Y.; Wang, J.; An, Q.; Liu, C.; Mai, L. Ultrathin $ZrO_2$ Coating Layer Regulates Zn Deposition and Raises Long-Life Performance of Aqueous Zn Batteries. *Mater. Today Energy* **2022**, *28*, 101056.
(38) Wang, L.; Huang, K.-W.; Chen, J.; Zheng, J. Ultralong Cycle Stability of Aqueous Zinc-Ion Batteries with Zinc Vanadium Oxide Cathodes. *Sci. Adv.* **2019**, *5* (10), eaax4279.
(39) Oberholzer, P.; Tervoort, E.; Bouzid, A.; Pasquarello, A.; Kundu, D. Oxide versus Nonoxide Cathode Materials for Aqueous Zn Batteries: An Insight into the Charge Storage Mechanism and Consequences Thereof. *ACS Appl. Mater. Interfaces* **2019**, *11* (1), 674−682.
(40) Ma, G.; Miao, L.; Dong, Y.; Yuan, W.; Nie, X.; Di, S.; Wang, Y.; Wang, L.; Zhang, N. Reshaping the Electrolyte Structure and Interface Chemistry for Stable Aqueous Zinc Batteries. *Energy Storage Mater.* **2022**, *47*, 203−210.
(41) Hao, J.; Yuan, L.; Ye, C.; Chao, D.; Davey, K.; Guo, Z.; Qiao, S.-Z. Boosting Zinc Electrode Reversibility in Aqueous Electrolytes by Using Low-Cost Antisolvents. *Angew. Chem., Int. Ed.* **2021**, *60* (13), 7366−7375.
(42) Zhao, M.; Rong, J.; Huo, F.; Lv, Y.; Yue, B.; Xiao, Y.; Chen, Y.; Hou, G.; Qiu, J.; Chen, S. Semi-Immobilized Ionic Liquid Regulator with Fast Kinetics toward Highly Stable Zinc Anode under −35 to 60 °C. *Adv. Mater.* **2022**, *34* (32), 2203153.
(43) Li, C.; Shyamsunder, A.; Hoane, A. G.; Long, D. M.; Kwok, C. Y.; Kotula, P. G.; Zavadil, K. R.; Gewirth, A. A.; Nazar, L. F. Highly Reversible Zn Anode with a Practical Areal Capacity Enabled by a Sustainable Electrolyte and Superacid Interfacial Chemistry. *Joule* **2022**, *6* (5), 1103−1120.
(44) Pei, A.; Zheng, G.; Shi, F.; Li, Y.; Cui, Y. Nanoscale Nucleation and Growth of Electrodeposited Lithium Metal. *Nano Lett.* **2017**, *17* (2), 1132−1139.
(45) Liu, W.; Liu, P.; Mitlin, D. Tutorial Review on Structure − Dendrite Growth Relations in Metal Battery Anode Supports. *Chem. Soc. Rev.* **2020**, *49* (20), 7284−7300.
(46) Yu, Z.; Rudnicki, P. E.; Zhang, Z.; Huang, Z.; Celik, H.; Oyakhire, S. T.; Chen, Y.; Kong, X.; Kim, S. C.; Xiao, X.; Wang, H.; Zheng, Y.; Kamat, G. A.; Kim, M. S.; Bent, S. F.; Qin, J.; Cui, Y.; Bao, Z. Rational Solvent Molecule Tuning for High-Performance Lithium Metal Battery Electrolytes. *Nat. Energy* **2022**, *7* (1), 94−106.
(47) Liu, H.; Sale, K. L.; Simmons, B. A.; Singh, S. Molecular Dynamics Study of Polysaccharides in Binary Solvent Mixtures of an Ionic Liquid and Water. *J. Phys. Chem. B* **2011**, *115* (34), 10251−10258.
(48) Ma, L.; Li, Q.; Ying, Y.; Ma, F.; Chen, S.; Li, Y.; Huang, H.; Zhi, C. Toward Practical High-Areal-Capacity Aqueous Zinc-Metal Batteries: Quantifying Hydrogen Evolution and a Solid-Ion Conductor for Stable Zinc Anodes. *Adv. Mater.* **2021**, *33* (12), 2007406.
(49) Yuvaraj, S. V. J.; Zhdanov, R. K.; Belosludov, R. V.; Belosludov, V. R.; Subbotin, O. S.; Kanie, K.; Funaki, K.; Muramatsu, A.; Nakamura, T.; Kawazoe, Y. Solvation Mechanism of Task-Specific Ionic Liquids in Water: A Combined Investigation Using Classical Molecular Dynamics and Density Functional Theory. *J. Phys. Chem. B* **2015**, *119* (40), 12894−12904.
(50) Niazi, A. A.; Rabideau, B. D.; Ismail, A. E. Effects of Water Concentration on the Structural and Diffusion Properties of Imidazolium-Based Ionic Liquid−Water Mixtures. *J. Phys. Chem. B* **2013**, *117* (5), 1378−1388.

(51) Peled, E.; Menkin, S. Review—SEI: Past, Present and Future. *J. Electrochem. Soc.* **2017**, *164* (7), A1703.
(52) Cheng, H.; Sun, Q.; Li, L.; Zou, Y.; Wang, Y.; Cai, T.; Zhao, F.; Liu, G.; Ma, Z.; Wahyudi, W.; Li, Q.; Ming, J. Emerging Era of Electrolyte Solvation Structure and Interfacial Model in Batteries. *ACS Energy Lett.* **2022**, *7* (1), 490−513.
(53) Brubach, J. B.; Mermet, A.; Filabozzi, A.; Gerschel, A.; Lairez, D.; Krafft, M. P.; Roy, P. Dependence of Water Dynamics upon Confinement Size. *J. Phys. Chem. B* **2001**, *105* (2), 430−435.
(54) Brubach, J.-B.; Mermet, A.; Filabozzi, A.; Gerschel, A.; Roy, P. Signatures of the Hydrogen Bonding in the Infrared Bands of Water. *J. Chem. Phys.* **2005**, *122* (18), 184509.
(55) Li, C.; Kingsbury, R.; Zhou, L.; Shyamsunder, A.; Persson, K. A.; Nazar, L. F. Tuning the Solvation Structure in Aqueous Zinc Batteries to Maximize Zn-Ion Intercalation and Optimize Dendrite-Free Zinc Plating. *ACS Energy Lett.* **2022**, *7* (1), 533−540.
(56) Ko, J. S.; Paul, P. P.; Wan, G.; Seitzman, N.; DeBlock, R. H.; Dunn, B. S.; Toney, M. F.; Nelson Weker, J. NASICON $Na_3V_2(PO_4)_3$ Enables Quasi-Two-Stage $Na^+$ and $Zn^{2+}$ Intercalation for Multivalent Zinc Batteries. *Chem. Mater.* **2020**, *32* (7), 3028−3035.
(57) Guo, G.; Tan, X.; Wang, K.; Zhang, H. High-Efficiency and Stable Zn-$Na_3V_2(PO_4)_3$ Aqueous Battery Enabled by Electrolyte-Induced Interphasial Engineering. *ChemSusChem* **2022**, *15* (11), e202200313.
(58) Zhang, H.; Tan, X.; Li, H.; Passerini, S.; Huang, W. Assessment and Progress of Polyanionic Cathodes in Aqueous Sodium Batteries. *Energy Environ. Sci.* **2021**, *14* (11), 5788−5800.
(59) Huang, Z.; Wang, T.; Song, H.; Li, X.; Liang, G.; Wang, D.; Yang, Q.; Chen, Z.; Ma, L.; Liu, Z.; Gao, B.; Fan, J.; Zhi, C. Effects of Anion Carriers on Capacitance and Self-Discharge Behaviors of Zinc Ion Capacitors. *Angew. Chem., Int. Ed.* **2021**, *60* (2), 1011−1021.
(60) Tang, H.; Yao, J.; Zhu, Y. Recent Developments and Future Prospects for Zinc-Ion Hybrid Capacitors: a Review. *Adv. Energy Mater.* **2021**, *11* (14), 2003994.